Equilenin-Derived DNA Adducts to Cytosine in DNA Duplexes: Structures and Thermodynamics†

Shuang Ding,‡ Robert Shapiro,‡ Nicholas E. Geacintov,‡ and Suse Broyde*,§

Department of Chemistry and Department of Biology, New York University, 100 Washington Square East, New York, New York 10003

Received June 8, 2005; Revised Manuscript Received September 21, 2005

ABSTRACT: The drug Premarin is the most widely used formula for hormone replacement therapy. However, long-term exposure to estrogens from the Premarin drug increases the risk of breast cancer. Equilin and equilenin, major components of Premarin, are predominantly metabolized to 4-hydroxyequilenin (4-OHEN). The quinoids produced by 4-OHEN oxidation react with dG, dA, and dC to form unusual stable cyclic bulky adducts, with four stereoisomers identified for each base adduct. The 4-OHEN−dC adducts are most predominant. They are mutagenic in vitro and have been found in human tumor tissue. We have carried out molecular modeling and molecular dynamics simulations to investigate structures and thermodynamics of the four 4-OHEN−dC stereoisomeric adducts in DNA duplexes. Our results show that the structure of each stereoisomer adduct in duplex DNA is specifically governed by its unique stereochemistry. The bulky adducts, with an obstructed Watson−Crick edge and an equilenin ring system near perpendicular to the damaged cytosine, are located in the B-DNA major or minor groove, with the modified cytosine in the *syn* or *anti* conformation, respectively. The DNA duplex structures are distorted, in terms of Watson−Crick pairing at and near the lesion, stacking interactions, and groove dimensions. Stereochemistry determines the orientation of the equilenin rings with respect to the 5′- to 3′-direction of the modified strand, as well as the positioning of the equilenin moiety's methyl and hydroxyl groups for each stereoisomer. The unusual structures and the stereochemical effects underlie their biological processing as miscoding DNA lesions whose mutagenic properties may contribute to breast cancer.

The drug Premarin is the most widely used formula for hormone replacement therapy (HRT). However, excessive exposure to estrogens through HRT has been determined to increase the risk of breast cancer (*1*−*3*). The nature of estrogen-induced carcinogenesis is complex and multifaceted, but one possible pathway for cancer initiation involves estrogen metabolism mediated by cytochrome P450 (*4*−*8*).

Premarin contains substantial amounts of equine estrogens, namely, equilin and equilenin. 4-Hydroxyequilenin (4-OHEN)[1] is the major phase I metabolite of both equilin and equilenin (*4*, *9*, *10*). This catechol estrogen autoxidizes to potent cytotoxic quinoids that cause a variety of DNA lesions (*8*, *11*, *12*). Though possible mechanisms whereby 4-OHEN may induce carcinogenesis are not fully understood, experimental evidence has shown that 4-OHEN induces various kinds of DNA damage in vitro and in vivo (*13*−*16*), including formation of unusual stable bulky adducts produced by alkylation (*14*). If not efficiently repaired by nucleotide excision repair or other repair mechanisms, the bulky lesions can cause mutations during DNA replication, which may initiate cancer (*17*).

The quinoids produced by 4-OHEN oxidation react with dG, dA, and dC to form unusual stable cyclic bulky adducts with guanine (4-OHEN−dG), cytosine (4-OHEN−dC), and adenine (4-OHEN−dA), but not thymine (*4*, *18*). Moreover, recently, such stable bulky adducts have been found in human breast cancer patients who use Premarin (*19*). The quinoid of 4-hydroxyequilin (4-OHEQ) from equilin metabolism oxidizes to 4-OHEN *o*-quinone and forms the same DNA adducts as 4-OHEN (*9*). 4-OHEQ has been shown to be mutagenic in a *supF* shuttle vector plasmid system propagated in human cells (*20*). Base substitutions of C·G pairs in the $^{5'}$-TC/AG-$^{5'}$ sequence were the predominant mutation observed, and the C·G → G·C and C·G → A·T transversions were attributed to a 4-OHEN−dC major adduct (*20*). In vitro primer extension studies conducted with several Y-family bypass polymerases, namely, Dpo4, pol η, and pol κ, indicate that the 4-OHEN−dC lesions can be bypassed with an incorrect dNTP or by slippage (*21*−*23*). It is most likely that the stereochemistry of the adducts, DNA sequence, and the type of polymerases involved in translesion bypass govern the specific nature and extent of these events.

The chemical structures of the 4-OHEN adducts have been determined (*18*, *24*), with four stereoisomers identified for each modified base (*25*). The Watson−Crick hydrogen

† This research is supported by NIH Grant CA-75449 to S.B., NIH Grant CA-73638 (subcontract from the University of Illinois at Chicago, J. Bolton, principal investigator), and NIH Grant CA-112412 to N.E.G.

* To whom correspondence should be addressed. Telephone: (212) 998-8231. Fax: (212) 995-4015. E-mail: broyde@nyu.edu.

‡ Department of Chemistry.

§ Department of Biology.

[1] Abbreviations: 4-OHEN, 4-hydroxyequilenin; 4-OHEN−C, 4-hydroxyequilenin−cytosine; 4-OHEQ, 4-hydroxyequilin; QM, quantum mechanics; DFT, density functional theory; MD, molecular dynamics; rmsd, root-mean-square deviations; MM-PBSA, molecular mechanics Poisson−Boltzmann surface area.

10.1021/bi051090t CCC: $30.25
Published on Web 10/14/2005

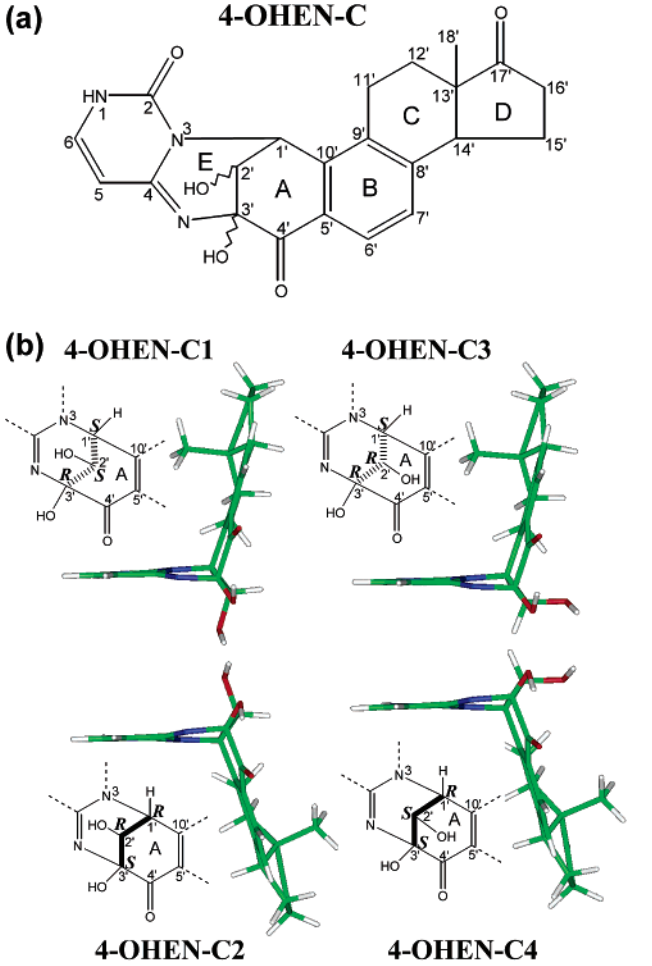

FIGURE 1: (a) Chemical structures and (b) quantum mechanical geometry-optimized conformations of 4-OHEN−C base adducts. (c) Sequence of the 11mer B-DNA duplex for the MD simulations. C* is the damaged cytosine.

bonding edge of the base is obstructed by the formation of the cyclic adduct in all cases. There are actually three chiral centers within the region connecting the nucleobase−4-OHEN ring system, and thus, the existence of eight stereoisomers is predicted (Figure 1a). However, stereoisomers containing the H and OH groups at the C1′ and C3′ positions in *trans* are not feasible due to the highly strained bridge ring in this configuration (*25*). Thus, only the stereochemistries at C2′ and C3′ determine the stereochemistry of the adducts, and therefore, there are only four stereoisomers.

The geometries and conformations of the four stereoisomeric 4-OHEN−C adducts on the base level (Figure 1b) have been previously determined by DFT quantum mechanical methods (*26*). The unsaturated bicyclo[3.3.1]nonane type linkage site causes the conformations of the 4-OHEN−C adducts to be severely restricted. Only one conformer was obtained for each adduct, in which the equilenin ring system is nearly perpendicular to the attached cytosine. The chirality of the C3′ atom determines the handedness of the 4-OHEN−C ring systems, and the C2′ chirality governs the orientation of its OH group. Stereochemically determined orientational differences of the equilenin ring system with respect to the base plane were noted, with the 4-OHEN−C1/C3 pair directed oppositely from the C2/C4 pair, as shown in Figure 1b.

In this work, we focus on determining the conformations of the four 4-OHEN−C stereoisomers in 11mer DNA duplexes with the sequence context defined in Figure 1c. This sequence was selected because it is under experimental investigation for physical and biochemical characterization. We employ computer modeling and molecular dynamics simulations to obtain trajectories, which provide ensembles for structural and thermodynamic analyses. Our results show that the covalently linked cytosine residue, with near-perpendicular equilenin rings rigidly linked to it, can adopt the *syn* or *anti* glycosidic bond conformations, placing the equilenin in the B-DNA major groove or minor groove, respectively. However, the adduct stereochemistry governs the specific orientation of each stereoisomer as well as the positioning of the equilenin C2′ OH and C18′ methyl groups. Moreover, the stereoisomeric lesions distort the DNA duplexes differentially. The unusual structural features of these four stereoisomeric 4-OHEN−dC adducts within the DNA duplexes may cause differences in their mutagenic and possibly carcinogenic activities.

METHODS

Starting Structures. A model of the unmodified sequence was created in a standard B-DNA conformation and energy minimized with DUPLEX (*27*). The C_7 residue was replaced with each of the four 4-OHEN−C adducts whose conformation had been computed by DFT optimization (*26*). The modified cytosine was rotated through the glycosidic torsion to locate conformations with minimal collisions. In each case, a narrow region in the *syn* domain of the glycosidic torsion was found (see Results). The equilenin moiety is located in the major groove (Figure S1a). For completion, we also investigated the *anti* conformational domain; here no structures without collision were obtained in the initial models. The fewest close contacts occurred when the equilenin was placed close to the Watson−Crick hydrogen bonding edge of an adjacent base pair (Figure S1b).

Force Field. The AMBER 8 molecular dynamics program package (*28*), the Cornell et al. force field (*29*), and the parm99.dat parameter set (*30*) were employed in performing MD. Force field parameters for 4-OHEN−C adducts that were not in the AMBER force field for proteins and nucleic acids were developed, consistent with the rest of the AMBER force field. Bond length, bond angle, and dihedral angle equilibrium values were taken from the DFT-optimized conformations. The force constants for bonds and angles were obtained by analogy with chemically similar atom types in the AMBER force field. The force constants for bond angles containing the N atom at the linkage site of the adduct (Figure 1a) were obtained through test calculations, which systematically varied these quantities until the QM-derived geometries at this atom in the rigid linkage region were maintained throughout the 5 ns MD simulations. The partial charges of the modified nucleotide were calculated with two stages of RESP in the AMBER package (*31*, *32*). Quantum mechanical Hartree−Fock calculations with the 6-31G* basis set using Guassian 98 (*33*) were first carried out. Then, the least-squares charge-fitting algorithm RESP (*32*, *34*) was used to

fit the derived electrostatic potentials to the atomic center of each molecule. Tables S1 and S2 (Supporting Information) give all the added force field parameters for the 4-OHEN−C stereoisomers.

Molecular Dynamics Protocol. The duplex starting model was neutralized with 20 Na^+ ions and solvated with explicit water using the LEAP module of AMBER. A periodic rectangular box of TIP3P water (*35*) with 10.0 Å buffer was created around the DNA. Table S3 gives the box sizes and numbers of the waters added in starting models. The particle-mesh Ewald (PME) (*36*, *37*) method with a 9.0 Å cutoff for the nonbonded interactions was used in the subsequent energy minimizations and dynamic simulations. Initially, 500 steps of steepest descent minimization followed by 500 steps of conjugate gradient minimization were conducted for the waters and sodium ions with 500 kcal mol^{-1} $Å^{-2}$ restraints placed on the DNA duplex. Then, 2000 steps of steepest descent minimization followed by 3000 steps of conjugate gradient minimization were carried out for the entire system without restraints. A 2 fs time step and the SHAKE algorithm (*38*) were applied in the MD simulations. The translational center-of-mass motion was removed every 2 ps (*39*). Visual inspection of the trajectories revealed no abnormal overall rotation of the DNA duplexes, indicating that energy leakage from internal motion to global rotation through the "flying ice cube effect" (*39*) was not contributing in this case. The system was heated from 0 to 293 K over 20 ps with a weak 10 kcal mol^{-1} $Å^{-2}$ restraint on the DNA at a constant volume, using the Berendsen coupling algorithm (*40*) with a 1.0 ps coupling parameter. The equilibration was continued with a further 100 ps of simulation without restraint at a constant atmospheric pressure, with a 2.0 ps coupling parameter. Finally, production was carried out for 5 ns at 293 K with a 4.0 ps heat bath coupling parameter. The temperature of 293 K was chosen because it is below the experimental thermal melting temperature (*61*).

Stability of the Molecular Dynamics Simulation. Plots of root-mean-square deviations (rmsd) of the current structure relative to the starting structure, as a function of time, are shown in Figure S2. The structures generally fluctuate stably after 2.5 ns, and our further analyses employ the 2.5−5 ns time frame.

Structural Analyses. The PTRAJ module of AMBER 8 and CARNAL of AMBER 7 (*41*) were employed for structural analyses. Stacking interactions were evaluated by computing the van der Waals interaction energies between adjacent base pairs, including the damaged cytosine and partner G pair, with the program ANAL of AMBER 8. The equilenin moiety, nearly perpendicular to the attached cytosine residue, is not included in the base stacking interaction. In addition, we employed a hydrogen bond quality index (*27*), I_H, to quantitatively assess the deviation from ideal Watson−Crick hydrogen bonding distances and angles for 5′- and 3′-side base pairs adjacent to the lesion:

$$I_H = \sum_{D-H\cdots A} [(d_{DA} - d^0{}_{DA})^2 + (1 + \cos\gamma)^2]$$

where d_{DA} is the instantaneous donor−acceptor distance, $d^0{}_{DA}$ is an ideal donor−acceptor distance [distances from N4 (C) to O6 (G) of 2.91 Å, from N1 (G) to N3 (C) of 2.95 Å, from N2 (G) to O2 (C) of 2.86 Å, from N6 (A) to O4 (T) of 2.95 Å, and from N1 (A) to N3 (T) of 2.82 Å] (*42*), and γ is the instantaneous D−H···A bond angle, with an ideal value of 180°. The summation is over all the Watson−Crick hydrogen bonds in a given pair and over 2.5−5 ns of the trajectory. I_H adopts a value of 0 when ideal Watson−Crick bonding is maintained. DNA duplex groove dimension information for the ensemble of structures of each stereoisomer was computed with MD Toolchest (*43*, *44*). We computed the bend angle of the duplex with CURVES (*43*), employing the "PP" option, which yields a bend angle measured between the vectors composed of the first two and last two reference points defining the axis. The first and last base pairs were removed prior to this analysis. In addition, we removed the modified cytosine since CURVES could not recognize this moiety. The computed bend angles were thus based on global helix axes determined by the four base pairs surrounding the lesion in each direction.

Free Energy Analyses. The molecular mechanics Poisson−Boltzmann surface area (MM-PBSA) (*45*−*51*) method in AMBER was employed for thermodynamic analyses. The free energies were estimated by averaging over 250 snapshots extracted at 10 ps intervals from the last 2.5 ns of the trajectory, with water molecules and counterions removed. The free energy, G, is computed from the molecular mechanical energy (E_{MM}), the solvation free energy ($G_{solvation}$), and the solute entropic contributions to free energy with the equation $G_{tot} = E_{MM} + G_{solvation} - T\Delta S$ (*45*, *46*). The molecular mechanical energy (E_{MM}) is calculated from internal energy (E_{int}) stemming from deviations of the bonds (E_{bonds}), angles (E_{angles}), and dihedral angles ($E_{dihedrals}$) from their equilibrium values, the van der Waals energy (E_{vdW}), and the electrostatic energy (E_{elect}). The same force field and parameters used in the MD simulations were applied to calculate the molecular mechanical energies (E_{MM}), but without cutoff for nonbonded interactions. The solvation free energy ($G_{solvation}$) is estimated from the electrostatic solvation energy (G_{PB}) and the nonpolar solvation energy ($G_{nonpolar}$). The electrostatic component of the solvation free energy is calculated with the Poisson−Boltzmann method using DelPhi (*52*, *53*). The temperature was set to 293 K, consistent with MD simulations. We used a probe radius of 1.4 Å to define the dielectric boundary, with atomic radii taken from the PARSE parameter set (*54*). The interior dielectric constant was set to 1, and the outside dielectric constant for the surrounding solvent was 80. The same partial charge set as in the MD simulations was employed. A physiological salt concentration of 0.15 M (*55*) was employed to model the effect of salt on the solvation free energy. For the Poisson−Boltzmann calculation, we applied a cubic lattice with a 0.5 Å grid spacing, in which the largest linear dimension of the molecule occupied 80% of the lattice. The boundary potential was approximated by the sum of the Debye−Huckel potentials of all the charges (*56*). Three hundred iterations using the linear PB equation followed by 1000 iterations with nonlinear PB equation were carried out. The nonpolar contribution of the solvation free energy is estimated with a surface-dependent area term by the equation $G_{nonpolar} = \gamma A + b$, where A is the solvent-accessible surface area (SASA) that is computed by Sanner's algorithm (*57*) in MSMS. γ and b are empirical constants, where $\gamma = 0.00542$ kcal/Å^2 and $b = 0.92$ kcal/mol (*54*).

The solute entropic contribution was approximated with normal mode calculations using the NMODE module (*45*, *46*) in the AMBER package, and 125 structures were selected at 20 ps intervals over the last 2.5 ns of the trajectory. Then, 1000 steps of steepest descent followed by conjugate gradient minimizations were carried out until the rmsd was less than 10^{-4} kcal mol^{-1} Å^{-1}. A distance-dependent dielectric constant ($\epsilon = 4r$, where r is the interatomic distance in angstroms) was used to mimic solvent effects. Then we selected the five minimized structures that had the lowest rmsd compared to the average structure to calculate the entropy, using the NMODE module of the AMBER 8 suite.

INSIGHT II from Accelrys, Inc., was employed for visualization and model building. Computations were carried out on our own cluster of Silicon Graphic Origin supercomputers and Octane workstations, as well as at the New York University Information Technology Services Origin supercomputer.

RESULTS AND DISCUSSION

We have carried out 5 ns MD simulations for the four 4-OHEN−C adducts within the 11mer duplex sequence given in Figure 1c, and analyzed the trajectories to obtain structural and thermodynamic properties of these modified duplexes. We began with the geometry-optimized structures of the four stereoisomeric 4-OHEN−C adducts that we had previously computed for the damaged bases (*26*). Each of these was modeled into an energy-minimized B-DNA duplex in the sequence of Figure 1c for the MD study. Both *syn* and *anti* glycosidic bond conformations were considered.

Starting Models

The first stage of this work required locating reasonable starting models for the MD simulations. Careful computer modeling involving continuous rotation about the glycosidic bond of the damaged cytosine in an energy-minimized B-DNA duplex showed only one region without any severe collisions for all four stereoisomers. In this conformation, the adduct was in the B-DNA major groove with the lesion glycosidic bond in the *syn* domain. For the *anti* models, the best initial structures all still had collisions, with the equilenin rings inserted into the duplex. Table S4 provides the starting values for the MD simulations of the glycosidic torsion χ for each stereoisomer in *syn* and *anti* glycosidic bond conformations. Figure S1 shows the starting models. The 5 ns molecular dynamics simulations performed from these starting models provided ensembles of structures, and the last 2.5 ns was used for detailed analyses.

Structural Analyses

Major and Minor Groove Structural Families. The *syn* and *anti* initial models provided major and minor groove conformational families for the equilenin ring system positioning (Figures 2 and S3). In the *syn* case, the initial models (Figure S1a) had equilenin rings in the major groove, nearly perpendicular to the damaged cytosine, which was partially stacked within the duplex. The emsemble derived from the MD simulations preserved these overall features. However, the best *anti* initial models (Figure S1b) had the equilenin rings inserted into the duplex with collisions; however, the dynamics relieved the initial collisions by repositioning the equilenin rings so that they protrude into the minor groove.

Adduct Stereochemistry Governs Structural Properties. The essential structural feature of all the equilenin-modified cytosines is the near-perpendicular orientation of the equilenin and bridge-linked cytosine, whose Watson−Crick edge is obstructed. This is true for each of the stereoisomeric adducts. However, stereochemistry plays an important role in determining the specific structural properties. Depending on the stereochemistry at the equilenin C3′ position and whether the glycosidic bond is *syn* or *anti*, the bulky ring system is 3′- or 5′-directed along the modified strand. Preliminary NMR data have also suggested opposite orientations of stereoisomers in duplex DNA (N. Zhang, A. Kolbanovskiy, S. Ding, A. Shastry, N. E. Geacintov, S. Broyde, and D. Patel, personal communication). Table 1 summarizes stereochemistry-determined structural features.

(i) Syn/Major Groove Conformation. With C3′ *R* stereochemistry in 4-OHEN−C1 and 4-OHEN−C3, the equilenin rings are oriented toward the 3′-direction of the modified strand (Figures 2a and 3a). However, with *S* stereochemistry at C3′, in 4-OHEN−C2 and 4-OHEN−C4, the equilenin rings are 5′-directed. Another structural feature that is determined by differences in stereochemistry of the four stereoisomeric adducts is the position of the C18′ methyl group. This group is directed inward toward the DNA and shielded from solvent in 4-OHEN−C1 and 4-OHEN−C3, with *R* stereochemistry at C3′. In the case of 4-OHEN−C2 and 4-OHEN−C4, with *S* stereochemistry at C3′, the hydrophobic methyl group is positioned outward from the DNA, exposed to solvent. In addition, the C2′ OH group orientation is governed by the combined stereochemistries at C2′ and C3′. In 4-OHEN−C1 and 4-OHEN−C2 with 2′*S*-3′*R* and 2′*R*-3′*S* stereochemistries, respectively, this OH group is nearly axial and oriented toward the modified strand. However, in 4-OHEN−C3 and −C4 with 2′*R*-3′*R* and 2′*S*-3′*S* stereochemistries, respectively, the OH group is nearly equatorial and outwardly directed into the solvent. The OH group at C3′ always points away from the equilenin rings and in the same direction as the bridge ring.

(ii) Anti/Minor Groove Conformation. With C3′ *R* stereochemistry in 4-OHEN−C1 and 4-OHEN−C3, the equilenin rings are oriented toward the 5′-direction of the modified strand, and the C18′ methyl group is directed toward the modified strand (Figures 2b and 3b). However, with *S* stereochemistry at C3′, in 4-OHEN−C2 and 4-OHEN−C4, the equilenin rings are 3′-directed and the methyl group is positioned toward the partner strand. In addition, for 4-OHEN−C1 and 4-OHEN−C2 with 2′*S*-3′*R* and 2′*R*-3′*S* stereochemistries, respectively, the C2′ OH group is nearly axial and solvent-exposed in the major groove. However, in 4-OHEN−C3 and −C4 with 2′*R*-3′*R* and 2′*S*-3′*S* stereochemistries, respectively, this OH group is nearly equatorial and directed toward the partner strand.

Hydrogen Bonding Interactions. The unique chemical structures of the 4-OHEN−C adducts afford opportunities for specific hydrogen bonds with DNA residues near the lesion, including the G partner base. Tables 2 and 3 summarize these interactions for both *syn* and *anti* conformations. These tables show that in the *anti*/minor groove conformation, the *anti* modified cytosine has a better opportunity to form hydrogen bonds with the partner and

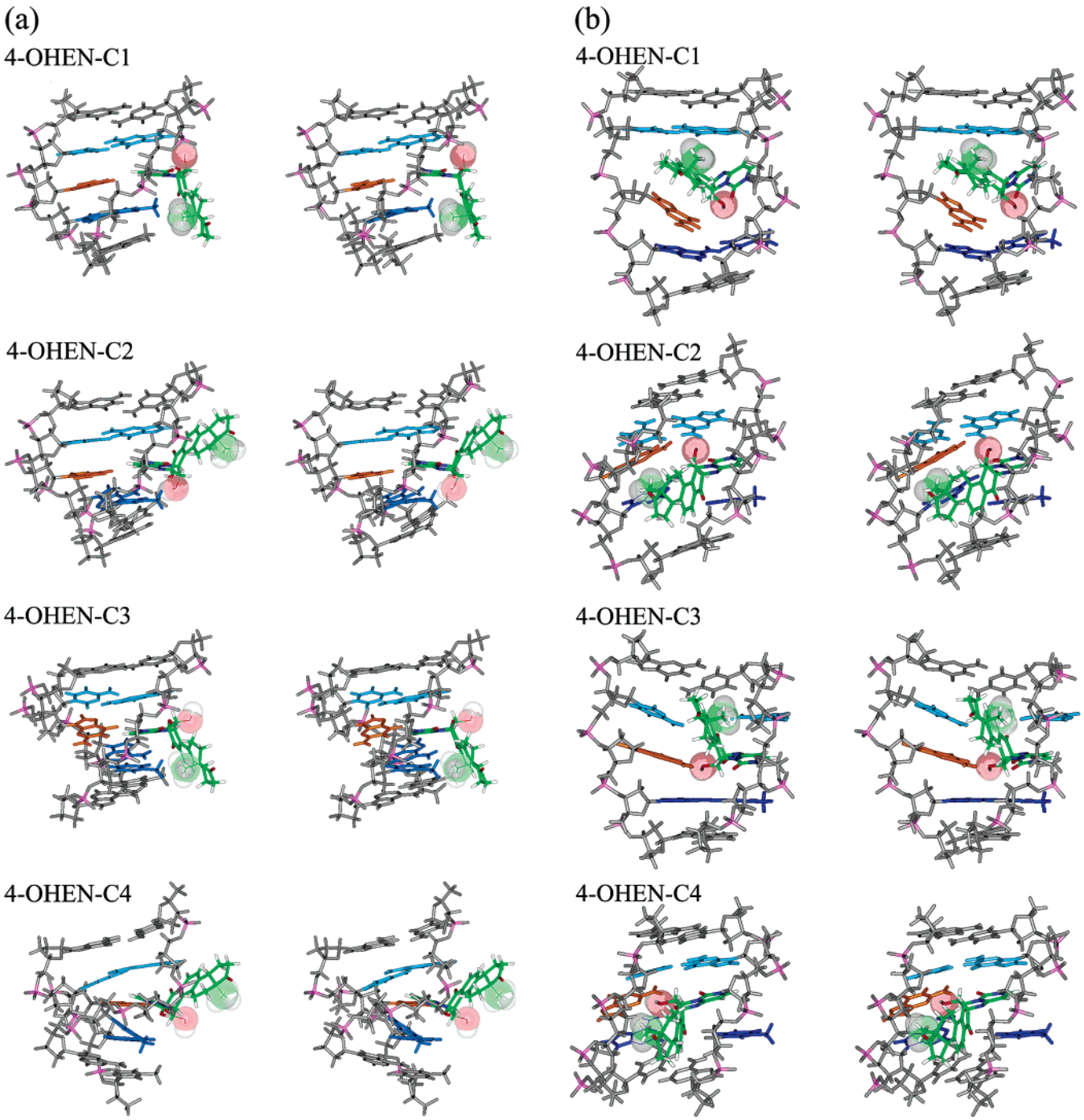

FIGURE 2: Central 5mers in the trajectory-average structures (2.5−5 ns) for the four 4-OHEN−C modified duplexes, in stereoview. The color code is as follows (4-OHEN−C, colored by atom): C, green; O, red; N, blue; H, white; partner base G, orange; 5′-side G_6•C_{17} pair, light blue; and 3′-side T_8•A_{15} pair, dark blue. The C2′ OH group of the adduct is shown as pink spheres and the C18′ methyl group as green spheres. All stereo images are constructed for viewing with a stereoviewer: (a) *syn*/major groove conformation and (b) *anti*/minor groove conformation.

Table 1: Stereochemistry-Determined Structural Properties of 4-OHEN−C Adducts

		syn/major groove conformation			*anti*/minor groove conformation		
	stereochemistry	equilenin rings[a]	C18′ methyl group[b,c]	C2′ OH group[b,c]	equilenin rings[a]	C18′ methyl group[c,d]	C2′ OH group[d,e]
4-OHEN−C1	2′*S*-3′*R*	3′	M	near-axial M	5′	M	near-axial SG
4-OHEN−C2	2′*R*-3′*S*	5′	S	near-axial M	3′	P	near-axial SG
4-OHEN−C3	2′*R*-3′*R*	3′	M	near-equatorial S	5′	M	near-equatorial P
4-OHEN−C4	2′*S*-3′*S*	5′	S	near-equatorial S	3′	P	near-equatorial P

[a] With respect to the modified strand. [b] S, toward solvent. [c] M, toward modified strand. [d] P, toward partner strand. [e] SG, solvent-exposed in major groove.

Table 2: Hydrogen Bonds and Occupancies Involving the Lesion C_7* or Partner G_{16} in the *Syn*/Major Groove Conformation[a]

	hydrogen bond	occupancy (%)
4-OHEN−C2	(C_7*) O2′−H···O4 (T_8)	52.8
4-OHEN−C3	(C_7*) O4′···H−N6 (A_{15})	39.5
	(T_8) O2···H−N2 (G_{16})	31.3
4-OHEN−C4	(C_7*) N···H−N2 (G_{16})	99.7
	(C_7*) O3′···H−N1 (G_{16})	89.3
	(T_8) O2···H−N2 (G_{16})	86.7

[a] Hydrogen bonding criteria were 3.35 Å between heavy atoms and a donor−hydrogen−acceptor hydrogen bonding angle of 135°. Data are for 2.5−5 ns.

Table 3: Hydrogen Bonds and Occupancies Involving the Lesion C_7* or Partner G_{16} in the *Anti*/Minor Groove Conformation[a]

	hydrogen bond	occupancy (%)
4-OHEN−C1	(T_8) O2···H−N2 (G_{16})	33.8
	(T_8) O2···H−N1 (G_{16})	31.3
4-OHEN−C2	(G_6) O6···H−N2 (G_{16})	24.1
	(C_7*) O3′···H−N6 (A_{15})	81.9
	(C_7*) O2′···H−N2 (G_{16})	33.9
	(C_7*) O4′···H−N2 (G_6)	44.9
	(G_{16}) N2−H···N3 (C_{17})	28.9
4-OHEN−C3	(C_7*) O2′···H−N2 (G_{16})	93.4
	(C_7*) O2′···H−N1 (G_{16})	79.4
	(C_7*) O4′···H−N2 (G_6)	81.3
4-OHEN−C4	(C_7*) O3′···H−N2 (G_{16})	93.8
	(C_7*) O2′−H···N3 (G_{16})	87.2
	(C_7*) O2′−H···N1 (A_{15})	26.6

[a] Hydrogen bonding criteria were 3.35 Å between heavy atoms and a donor−hydrogen−acceptor hydrogen bonding angle of 135°. Data are for 2.5−5 ns.

adjacent bases. This stems from the fact that the bridge ring is directed inward toward the partner strand in the *anti* conformers, rather than toward solvent as in the *syn*/major groove case (Figure 2). Interestingly, 4-OHEN−C1 does not participate in any hydrogen bonds in either the *syn* or the *anti* conformation.

(i) Syn/Major Groove Conformation. Watson−Crick hydrogen bond occupancies of base pairs adjacent to the lesion and beyond are greater than 90% (Table S5) in every case, except at the ends, and for the T_8·A_{15} pair in 4-OHEN−C4. However, these hydrogen bonds are in some cases very perturbed adjacent to the lesion. Specifically, our hydrogen bond quality index (see Methods) shows that the most notable distortion is found in 4-OHEN−C4 at the T_8·A_{15} pair on the 3′-side of the damage (Figure 4a). In the 4-OHEN−C4 case, this stems from abnormal hydrogen bond interactions between G_{16} and the C_7* linkage bridge, as well as with T_8 (Table 2), which distorts the T_8·A_{15} base pair 3′ to the lesion. In these *syn* conformations, the base pairing perturbations are most significant in the 4-OHEN−C3 and −C4 cases (Figure 4a), at the base pair opposite to the equilenin directionality, and are caused by specific hydrogen bonds between the equilenin or G_{16} and the T_8·A_{15} base pair.

(ii) Anti/Minor Groove Conformation. For 4-OHEN−C1, Watson−Crick hydrogen bonds are maintained in all base pairs except at the lesion site, but the hydrogen bond quality index shows that the T_8·A_{15} pair on the 3′-side of the damage is disturbed: the occupancy for one of the Watson−Crick hydrogen bonds of the T_8·A_{15} pair is only 75% (Table S5). The origin of this perturbation is discussed below. Watson−Crick hydrogen bonds are completely disrupted on the 3′-side base pair (T_8·A_{15}) of 4-OHEN−C2 and 4-OHEN−C4, and the 5′-side (G_6·C_{17}) of 4-OHEN−C3 (Figure 4b). Thus, the direction of the equilenin rings parallels the direction of the disrupted base pair in the *anti* conformations of 4-OHEN−C2, −C3, and −C4.

Base Stacking Interactions. In both major and minor groove conformations, the adducts cause alterations in the stacking interactions of the B-DNA duplex compared to the unmodified system. The modified cytosine and its partner G_{16} are not stacked normally, in line with the absence of Watson−Crick hydrogen bonding at the lesion. A partial energetic assessment of differential stacking interactions can be obtained from van der Waals interactions between base pairs. The van der Waals energies provide just one important energetic component contributing to stacking stabilization; however, the results show uniformly that the modified duplexes are less stabilized by stacking through van der Waals interactions than the unmodified one. Figure 5 and Table S6 show these van der Waals interaction energies, and clearly reveal the weakened stacking in every case. This disturbed stacking radiates beyond the damage site in both directions.

(i) Syn/Major Groove Conformation. C_7* is mainly stacked within the B-DNA duplex. However, the most prominent weakening of stacking interactions involves the damaged cytosine and its partner for each stereoisomer. Disturbance of the stacking interactions is greatest in 4-OHEN−C4, due to its unusual hydrogen bonding interactions (Table 2), while the other three stereoisomeric adducts have similar extents of perturbation.

(ii) Anti/Minor Groove Conformation. The modified cytosine is also mainly stacked within the helix, except for 4-OHEN−C1. In this case, the modified cytosine is tilted ∼60° with respect to the adjacent bases and the aromatic equilenin B ring stacks with the partner base G_{16}; consequently, G_{16} is 3′-directed along the modified strand, and stacks only slightly with A_{15}. This also causes the disruption of the hydrogen bond in the T_8·A_{15} pair, described above. The disturbance of stacking interactions is greatest for 4-OHEN−C1 (Figure 5b). In the case of the other three stereoisomers, because Watson−Crick hydrogen bonds are disrupted in the base pair adjacent to the lesion, the greatest weakening of stacking involves the disrupted base pair, namely, the 5′-side base pair (G_6·C_{17}) of 4-OHEN−C3 and the 3′-side base pair (T_8·A_{15}) of 4-OHEN−C2 and −C4.

Groove Dimensions. The accommodation of the bulky 4-OHEN−C adducts in the major or minor groove perturbs groove dimensions of the B-DNA duplex (Figure 6).

(i) Syn/Major Groove Conformation. The positioning of the equilenin moiety in the B-DNA major groove narrows this groove on the 5′-side and enlarges it on the 3′-side of the modified strand for all stereoisomers. Only 4-OHEN−C4 also shows enlargement across P5−P15, which likely is associated with its 5′-orientation. However, 4-OHEN−C2, also 5′-directed, does not show any P5−P15 enlargement because it compresses the major groove and expands somewhat the minor groove, due to a greater bend (see below). For 4-OHEN−C1, the minor grooves are close to normal. Also of note is the narrowing of the minor groove in 4-OHEN−C3 and 4-OHEN−C4, resulting from the cross-strand hydrogen bond between G_{16} and T_8, which tends to narrow the groove. In 4-OHEN−C4, the hydrogen bond

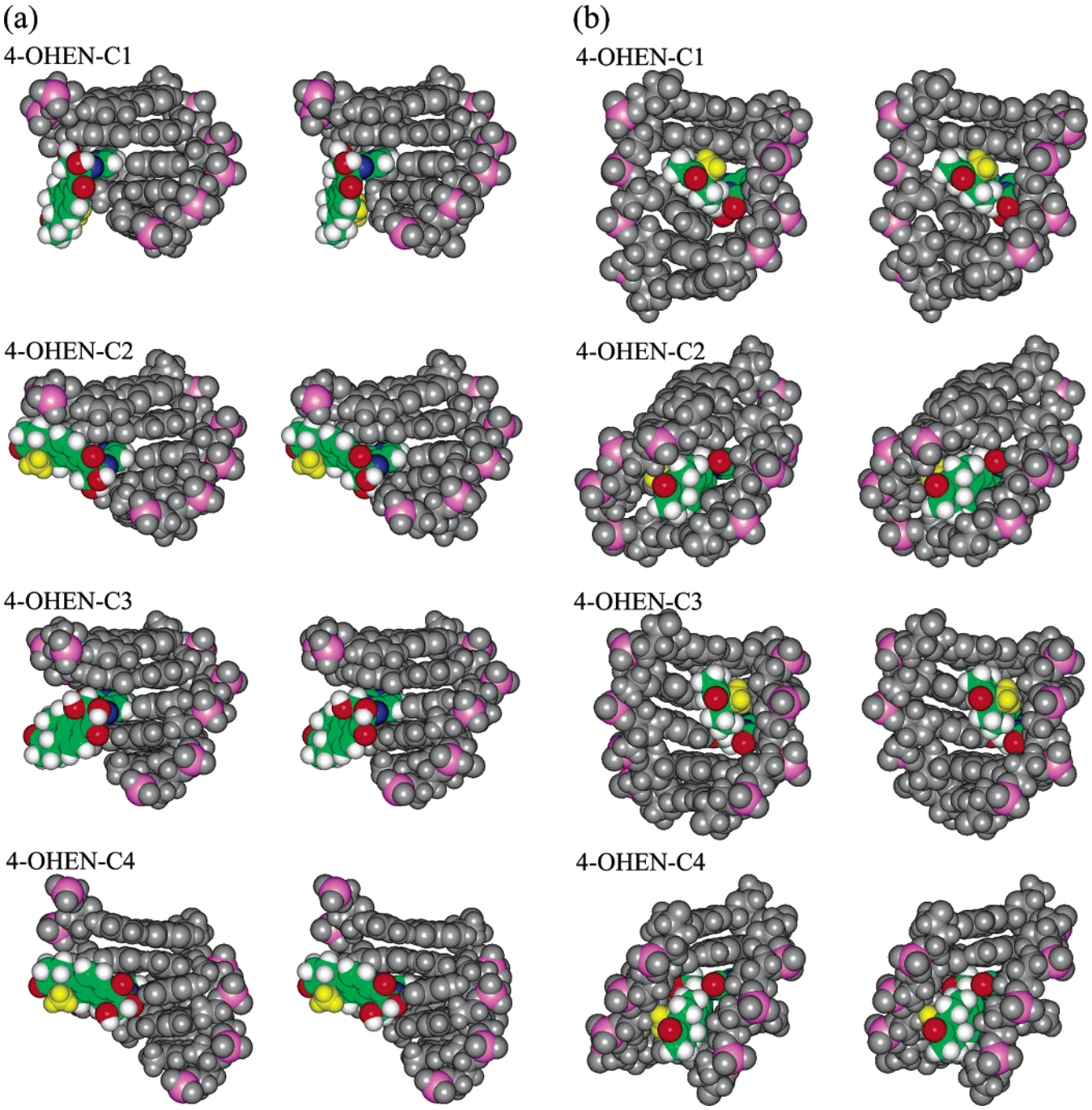

FIGURE 3: Space filling models of central 5mers in the trajectory-average structures (2.5−5 ns) for the four 4-OHEN−C modified duplexes, in stereoview. The color code is as follows (4-OHEN−C, colored by atom): C, green; O, red; N, blue; and H, white (except the methyl group is yellow). (a) *syn*/major groove conformation and (b) *anti*/minor groove conformation.

between T_8 and G_{16} forces the backbone adjacent to T_8 very close to the partner strand, with a severe narrowing of the minor groove. The stereoisomer which most distorts both the major and the minor groove is 4-OHEN−C4. The unusual hydrogen bond between T_8 and G_{16} (Table 2) is responsible for these perturbations.

(ii) Anti/Minor Groove Conformation. For 4-OHEN−C1 and −C3, the minor groove positioning of the equilenin moiety greatly opens this groove, which is likely associated with the 5′-orientation of these adducts. For the 3′-directed 4-OHEN−C2 and −C4, the minor grooves are close to normal. Also of note is the enlargement of the major groove in all four stereoisomers, but more so in C1 and C2. 4-OHEN−C3 and −C4 have less major groove opening compared to the unmodified duplex, possibly resulting from the stronger bending (see below), which tends to close the groove. The most groove-distorting stereoisomer is 4-OHEN−C1, due to the unusual stacking between the aromatic B ring of equilenin moiety and partner base G_{16}.

Bending. Our analyses of bending in the damaged duplexes reveal that stereochemistry and conformation determine the extent and flexibility of adduct-induced bends.

(i) Syn/Major Groove Conformation. Bending in the 4-OHEN−C3 and −C4 adducts is modest and comparable to that of the unmodified control duplex. However, 4-OHEN−C1 and −C2 are more bent. The bends are into the major groove, and are quite flexible (Figure S4a). It appears that the near axial C2′ OH group with its proximity to the

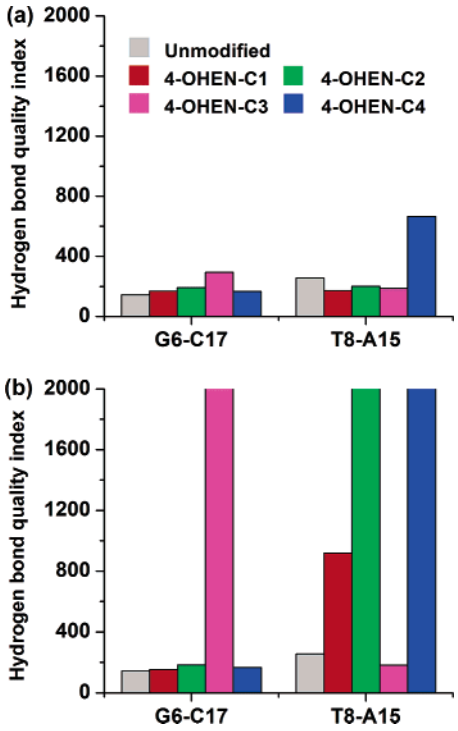

FIGURE 4: Trajectory-summed hydrogen bond quality index (2.5−5 ns) for 5′- and 3′-side base pairs adjacent to the lesion and defined in Figure 1: (a) *syn*/major groove conformation and (b) *anti*/minor groove conformation. The quality indexes for the G_6•C_{17} pair of 4-OHEN−C3 and the T_8•A_{15} pair of 4-OHEN−C2 and −C4 are 533 790, 86 780, and 296 878, respectively, indicating complete rupture.

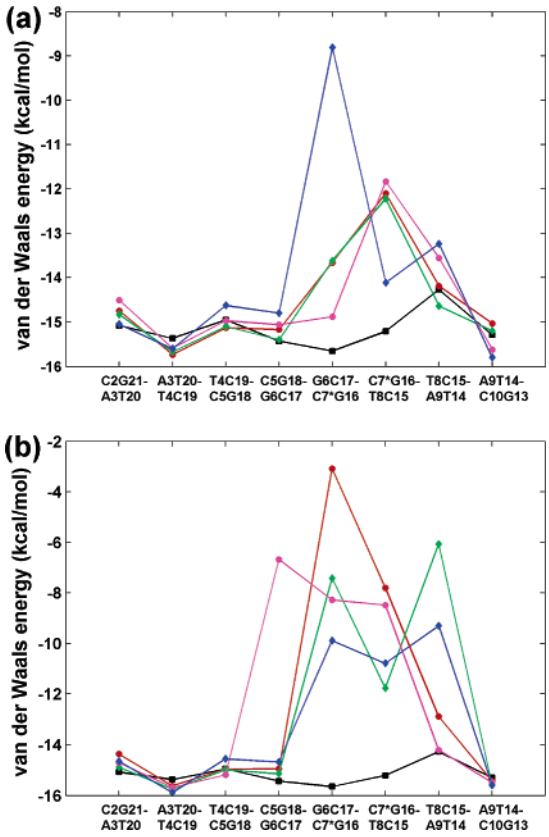

FIGURE 5: Trajectory-average van der Waals interaction energy (2.5−5 ns) vs base pair step plot. The color code is as follows: 4-OHEN−C1, red; 4-OHEN−C2, green; 4-OHEN−C3, magenta; 4-OHEN−C4, blue; and unmodified duplex, black. (a) *syn*/major groove conformation and (b) *anti*/minor groove conformation.

modified strand in the major groove facilitates this bending in C1 and C2. In the case of C2, the hydrogen bond between the C2′ OH group and O4 of the T_8 base may contribute to facilitating the bend. In the case of C1, the situation is more complex. No specific hydrogen bond is formed between the C2′ OH group and any DNA acceptor. However, throughout the trajectory, two atoms of DNA, namely, C8 and N7 of G_6, come very close to C2′ O (3.3 ± 0.2 and 3.6 ± 0.4 Å, respectively). Fluctuating electrostatic and steric interactions due to these close encounters likely produce the fluctuating bends apparent in the MD simulation trajectories.

(ii) Anti/Minor Groove Conformation. Bends are quite flexible, and the bending is more significant, except for C1 which is comparable to the unmodified duplex (Figure S4b). It appears that cross-strand hydrogen bonds between the adduct and adjacent bases may contribute to facilitating the bends. Hydrogen bonds between the modified cytosine and the partner base G_{16} (Table 3) support the large bend in 4-OHEN−C3 and −C4. 4-OHEN−C2 forms a hydrogen bond with adjacent base A_{15} (occupancy of 82%), as well as weaker hydrogen bonding with partner base G_{16} (34%) and adjacent G_6 (45%). In the case of 4-OHEN−C1, there is no hydrogen bonding involving this adduct, but the unusual stacking greatly opens both grooves and impedes bending (Figure S3).

Helix Destabilization

Experimental thermal melting data in the same sequence context indicate that these adducts are quite destabilizing (∼20°) compared to unmodified DNA (*61*), consistent with our structural analyses. Table 4 summarizes structural perturbations that can account for the destabilization. These include perturbed stacking, disturbed Watson−Crick hydrogen bonding at and adjacent to the lesion, and major and minor groove distortions.

Thermodynamic Analyses

The ensemble of structures derived from the MD simulations were employed to carry out thermodynamic analyses of the simulated structures, using the MM-PBSA method (*45*−*51*). To compare stabilities of the major and minor groove conformational families, we calculated the relative free energies, Δ*G*, for the *syn* and *anti* conformations. Table S7 gives the full thermodynamic analyses, and Table 5 gives relative stabilities. Energy differences between the families, particularly for 4-OHEN−C1 and −C2, are not great, suggesting that either family may be possible, depending possibly on environmental conditions and base sequence context. However, preferences for the major and minor groove conformations appear to be somewhat greater for 4-OHEN−C3 and −C4, respectively.

Biological Implications

The unique structural and stereochemical properties of these 4-OHEN lesions in DNA duplexes would adversely impact cellular DNA functioning in replication and transcription. The obstructed Watson−Crick edge in the damaged cytosine itself predicts that replication may be mutagenic. In addition, the rigidly connected equilenin rings perpendicular to the cytosine create a highly inflexible and bulky

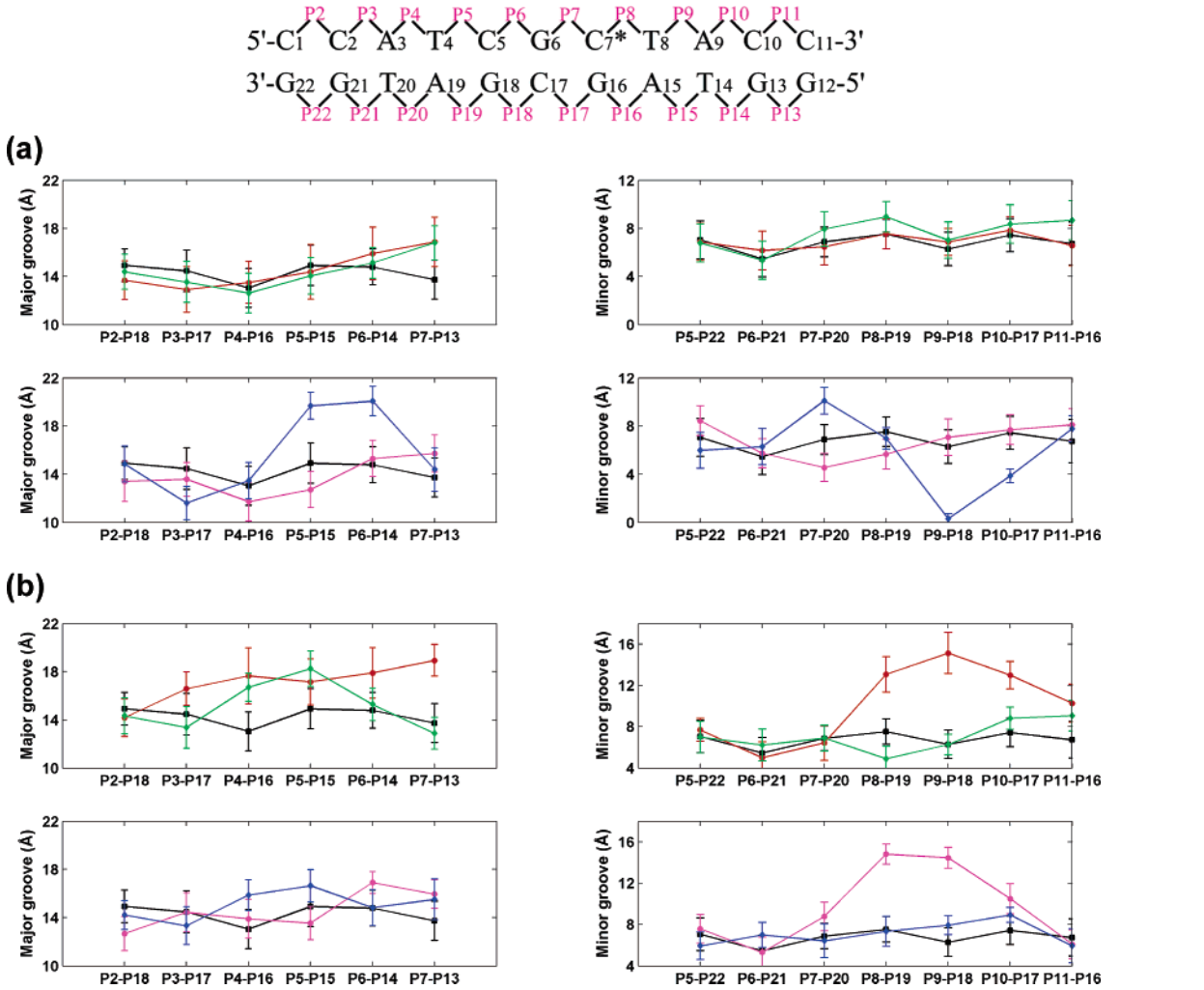

FIGURE 6: Trajectory-average groove dimensions (2.5−5 ns) of 4-OHEN−C modified duplexes. The color code is the same as in Figure 4: (a) *syn*/major groove conformation and (b) *anti*/minor groove conformation.

Table 4: Distortions in 4-OHEN−C Modified Duplexes

			stereoisomer			
		unmodified	C1	C2	C3	C4
		Syn/Major Groove Conformation				
Watson−Crick	G_6•C_{17}	298.7	297.7	296.1	292.2	298.5
hydrogen bond	C_7*•G_{16}	298.0	0.0	0.0	0.0	0.0
occupancy[a] (%)	T_8•A_{15}	188.4	195.7	192.8	196.2	177.0
stacking[b] (kcal/mol)		−121.3	−115.8	−116.7	−116.0	−112.1
bend angle[c] (deg)		15.5	27.4	26.5	14.8	15.6
groove distortion[d] (Å)		0.0	3.1 (M)	3.1 (M)	−2.3 (m)	−6.0 (m)
		Anti/Minor Groove Conformation				
Watson−Crick	G_6•C_{17}	298.7	287.8	297.1	0.0	298.1
hydrogen bond	C_7*•G_{16}	298.0	0.0	0.0	0.0	0.0
occupancy[a] (%)	T_8•A_{15}	188.4	167.8	0.0	196.9	0.0
stacking[b] (kcal/mol)		−121.3	−99.1	−101.6	−98.7	−105.4
bend angle[c] (deg)		15.5	19.6	31.3	53.9	55.6
groove distortion[d] (Å)		0.0	8.8 (m)	3.7 (M)	8.2 (m)	2.8 (M)

[a] Summed over all the Watson−Crick hydrogen bonds in a given pair. [b] Stacking interactions are sums of van der Waals interaction energies over all base pairs in each duplex, except for the base pair at each end of the duplex (Table S6). [c] The bend angle is the trajectory-average value over 2.5−5 ns (Figure S4). [d] Using the unmodified duplex as a reference, we calculated the distortions of the 4-OHEN−C modified duplexes as $d - d_0$, where d is a groove dimension of the 4-OHEN−C modified duplex and d_0 is the corresponding value for the unmodified duplex. For each conformation, all minor and major groove dimensions were compared with those of the unmodified duplex (data from Figure 6), and the one with the largest absolute value is shown. M and m designate the major and minor groove, respectively.

group which would be expected to severely perturb the normal positions of neighboring amino acid residues in polymerases, particularly at the tightly fitting active site of a replicative DNA polymerase ternary complex (*58*). Experimental evidence from in vitro primer extension studies has shown blockage by a replicative pol α polymerase, consistent with active site distortion, as well as mutagenic bypass in this and in several error prone bypass polymerases

Table 5: Relative Free Energies for *Syn*/Major Groove and *Anti*/Minor Groove Conformations[a]

	ΔG (kcal/mol)			
stereoisomer	C1	C2	C3	C4
syn/major groove	0.0	3.9	0.0	5.0
anti/minor groove	1.5	0.0	6.8	0.0

[a] For each stereoisomeric adduct, the conformation with the lower energy is assigned a ΔG of 0.

(*21*−*23*). Furthermore, stereoisomer-dependent differences in treatment of these lesions by DNA polymerases have been observed experimentally (*21*−*23*), and are most likely governed by the orientational differences between the four stereoisomeric adducts. The opposite orientations of stereoisomer pairs of adducts along the modified strand are likely to play an important part in the differential treatment by polymerases, analogous to the case of oppositely oriented polycyclic aromatic hydrocarbon-derived adducts (*59*, *60*). Finally, the predicted differences in the structural properties of the four stereoisomeric adducts may give rise to differences in their rates of excision by DNA repair enzymes.

CONCLUSION

The 4-OHEN−C adducts are rigid lesions with obstructed Watson−Crick edges and nearly perpendicular ring systems. The four 4-OHEN−C stereoisomeric adducts can reside in the B-DNA major groove with *syn* damaged cytosine or minor groove with *anti* damaged cytosine. In each structural family opposite orientation of the equilenin ring system, the C18′ bulky methyl group and the bridge ring C2′ OH group are found. The lesions cause distortions involving disruption of Watson−Crick hydrogen bonding at the lesion and adjacent sites, perturbed stacking, and distorted groove dimensions, consistent with observed thermal melting destabilization. The unique structural properties of the 4-OHEN−C adducts and the profound stereochemically governed differences among them likely underlie their mutagenic and possibly tumorigenic properties.

SUPPORTING INFORMATION AVAILABLE

Table S1 gives AMBER atom type, connection type, and partial charge assignments for 4-OHEN−C adducts. Table S2 gives added force field parameters for the modified cytosine. Table S3 gives box sizes and numbers of waters added to the MD simulation starting models. Table S4 gives glycosidic torsion χ values in the starting structures. Table S5 gives Watson−Crick hydrogen bonds and occupancies in 4-OHEN−C modified duplexes. Table S6 gives van der Waals interactions between the base pairs. Table S7 gives MM-PBSA free energy components for 4-OHEN−C modified duplexes. Figure S1 shows starting structures for the MD simulations. Figure S2 shows rmsd versus time plots for each molecular dynamics simulation. Figure S3 shows trajectory-average structures of 4-OHEN−C modified DNA duplexes. Figure S4 shows bend angle versus time plots for each molecular dynamics simulation. This material is available free of charge via the Internet at http://pubs.acs.org.

REFERENCES

1. Liehr, J. G. (1990) Genotoxic effects of estrogens, *Mutat. Res. 238*, 269−76.
2. Colditz, G. A., Hankinson, S. E., Hunter, D. J., Willett, W. C., Manson, J. E., Stampfer, M. J., Hennekens, C., Rosner, B., and Speizer, F. E. (1995) The use of estrogens and progestins and the risk of breast cancer in postmenopausal women, *N. Engl. J. Med. 332*, 1589−93.
3. Feigelson, H. S., and Henderson, B. E. (1996) Estrogens and breast cancer, *Carcinogenesis 17*, 2279−84.
4. Bolton, J. L., Pisha, E., Zhang, F., and Qiu, S. (1998) Role of quinoids in estrogen carcinogenesis, *Chem. Res. Toxicol. 11*, 1113−27.
5. Service, R. F. (1998) New role for estrogen in cancer? *Science 279*, 1631−3.
6. Yager, J. D., and Liehr, J. G. (1996) Molecular mechanisms of estrogen carcinogenesis, *Annu. Rev. Pharmacol. Toxicol. 36*, 203−32.
7. Zhu, B. T., and Conney, A. H. (1998) Functional role of estrogen metabolism in target cells: Review and perspectives, *Carcinogenesis 19*, 1−27.
8. Bolton, J. L. (2002) Quinoids, quinoid radicals, and phenoxyl radicals formed from estrogens and antiestrogens, *Toxicology 177*, 55−65.
9. Zhang, F., Chen, Y., Pisha, E., Shen, L., Xiong, Y., van Breemen, R. B., and Bolton, J. L. (1999) The major metabolite of equilin, 4-hydroxyequilin, autoxidizes to an o-quinone which isomerizes to the potent cytotoxin 4-hydroxyequilenin-o-quinone, *Chem. Res. Toxicol. 12*, 204−13.
10. Chang, M., Zhang, F., Shen, L., Pauss, N., Alam, I., van Breemen, R. B., Blond, S. Y., and Bolton, J. L. (1998) Inhibition of glutathione S-transferase activity by the quinoid metabolites of equine estrogens, *Chem. Res. Toxicol. 11*, 758−65.
11. Bolton, J. L., Trush, M. A., Penning, T. M., Dryhurst, G., and Monks, T. J. (2000) Role of quinones in toxicology, *Chem. Res. Toxicol. 13*, 135−60.
12. Shen, L., Pisha, E., Huang, Z., Pezzuto, J. M., Krol, E., Alam, Z., van Breemen, R. B., and Bolton, J. L. (1997) Bioreductive activation of catechol estrogen-ortho-quinones: Aromatization of the B ring in 4-hydroxyequilenin markedly alters quinoid formation and reactivity, *Carcinogenesis 18*, 1093−101.
13. Li, Y., Yao, J., Chang, M., Cuendet, M., and Bolton, J. L. (2004) Altered apoptotic response in MCF 10A cells treated with the equine estrogen metabolite, 4-hydroxyequilenin, *Toxicol. Lett. 154*, 225−33.
14. Zhang, F., Swanson, S. M., van Breemen, R. B., Liu, X., Yang, Y., Gu, C., and Bolton, J. L. (2001) Equine estrogen metabolite 4-hydroxyequilenin induces DNA damage in the rat mammary tissues: Formation of single-strand breaks, apurinic sites, stable adducts, and oxidized bases, *Chem. Res. Toxicol. 14*, 1654−9.
15. Chen, Y., Liu, X., Pisha, E., Constantinou, A. I., Hua, Y., Shen, L., van Breemen, R. B., Elguindi, E. C., Blond, S. Y., Zhang, F., and Bolton, J. L. (2000) A metabolite of equine estrogens, 4-hydroxyequilenin, induces DNA damage and apoptosis in breast cancer cell lines, *Chem. Res. Toxicol. 13*, 342−50.
16. Pisha, E., Lui, X., Constantinou, A. I., and Bolton, J. L. (2001) Evidence that a metabolite of equine estrogens, 4-hydroxyequilenin, induces cellular transformation in vitro, *Chem. Res. Toxicol. 14*, 82−90.
17. Loechler, E. L. (1996) The role of adduct site-specific mutagenesis in understanding how carcinogen-DNA adducts cause mutations: Perspective, prospects and problems, *Carcinogenesis 17*, 895−902.
18. Shen, L., Qiu, S., Chen, Y., Zhang, F., van Breemen, R. B., Nikolic, D., and Bolton, J. L. (1998) Alkylation of 2′-deoxynucleosides and DNA by the Premarin metabolite 4-hydroxyequilenin semiquinone radical, *Chem. Res. Toxicol. 11*, 94−101.
19. Embrechts, J., Lemiere, F., Van Dongen, W., Esmans, E. L., Buytaert, P., Van Marck, E., Kockx, M., and Makar, A. (2003) Detection of estrogen DNA-adducts in human breast tumor tissue and healthy tissue by combined nano LC-nano ES tandem mass spectrometry, *J. Am. Soc. Mass Spectrom. 14*, 482−91.
20. Yasui, M., Matsui, S., Laxmi, Y. R., Suzuki, N., Kim, S. Y., Shibutani, S., and Matsuda, T. (2003) Mutagenic events induced by 4-hydroxyequilin in supF shuttle vector plasmid propagated in human cells, *Carcinogenesis 24*, 911−7.

21. Suzuki, N., Yasui, M., Santosh Laxmi, Y. R., Ohmori, H., Hanaoka, F., and Shibutani, S. (2004) Translesion synthesis past equine estrogen-derived 2′-deoxycytidine DNA adducts by human DNA polymerases *η* and *κ*, *Biochemistry 43*, 11312−20.
22. Chen, D. D., Oum, L., Kolbanovskiy, A., Kuzmin, V., Shastry, A., Chang, M. S., Bolton, J. L., and Geacintov, N. (2004) Translesion synthesis and nucleotide excision repair of site specifically modified oligodeoxyribonucleotides containing single lesions derived from the equine estrogen metabolite 4-OHEN, *Chem. Res. Toxicol. 17*, 1782.
23. Geacintov, N. E., Kolbanovskiy, A., Kuzmin, K., Chang, M. S., and Bolton, J. L. (2003) DNA damage induced by an equine estrogen metabolite (4-OHEN) in solution and the characteristics of site specifically modified oligodeoxynucleotide model systems containing single, stable covalent adducts, *Chem. Res. Toxicol. 16*, 1665−6.
24. Shen, L., Qiu, S. X., vanBreemen, R. B., Zhang, F. G., Chen, Y. M., and Bolton, J. L. (1997) Reaction of the Premarin metabolite 4-hydroxyequilenin semiquinone radical with 2′-deoxyguanosine: Formation of unusual cyclic adducts, *J. Am. Chem. Soc. 119*, 11126−7.
25. Embrechts, J., Lemiere, F., Van Dongen, W., and Esmans, E. L. (2001) Equilenin-2′-deoxynucleoside adducts: Analysis with nano-liquid chromatography coupled to nano-electrospray tandem mass spectrometry, *J. Mass Spectrom. 36*, 317−28.
26. Ding, S., Shapiro, R., Geacintov, N. E., and Broyde, S. (2003) Conformations of stereoisomeric base adducts to 4-hydroxyequilenin, *Chem. Res. Toxicol. 16*, 695−707.
27. Hingerty, B. E., Figueroa, S., Hayden, T. L., and Broyde, S. (1989) Prediction of DNA structure from sequence: A build-up technique, *Biopolymers 28*, 1195−222.
28. Case, D. A., Darden, T. A., Cheatham, T. E., III, Simmerling, C. L., Wang, J., Duke, R. E., Luo, R., Merz, K. M., Wang, B., Pearlman, D. A., Crowley, M., Brozell, S., Tsui, V., Gohlke, H., Mongan, J., Hornak, V., Cui, G., Beroza, P., Schafmeister, C., and Kollman, P. A. (2004) *AMBER 8*, University of California, San Francisco.
29. Cornell, W. D., Cieplak, P., Bayly, C. I., Gould, I. R., Merz, K. M., Ferguson, D. M., Spellmeyer, D. C., Fox, T., Caldwell, J. W., and Kollman, P. A. (1995) A 2nd Generation Force-Field for the Simulation of Proteins, Nucleic-Acids, and Organic-Molecules, *J. Am. Chem. Soc. 117*, 5179−97.
30. Cheatham, T. E., Cieplak, P., and Kollman, P. A. (1999) A modified version of the Cornell et al. force field with improved sugar pucker phases and helical repeat, *J. Biomol. Struct. Dyn. 16*, 845−62.
31. Zhang, Q., Broyde, S., and Schlick, T. (2004) Deformations of promoter DNA bound to carcinogens help interpret effects on TATA-element structure and activity, *Philos. Trans. R. Soc. London, Ser. A 362*, 1479−96.
32. Cieplak, P., Cornell, W. D., Bayly, C., and Kollman, P. A. (1995) Application of the Multimolecule and Multiconformational Resp Methodology to Biopolymers: Charge Derivation for DNA, RNA, and Proteins, *J. Comput. Chem. 16*, 1357−77.
33. Frisch, J. M., Trucks, W. G., Schlegel, B. H., Scuseria, E. G., Robb, A. M., Cheeseman, R. J., Zakrzewski, G. V., Montgomery, A. J., Stratmann, E. R., Burant, C. J., Dappprich, S., Millam, M. J., Daniels, D. A., Kudin, N. K., Strain, C. M., Farkas, O., Tomasi, J., Barone, V., Cossi, M., Cammi, R., Mennucci, B., Pomelli, C., Adamo, C., Clifford, S., Ochterski, J., Petersson, A. G., Ayala, Y. P., Cui, Q., Morokuma, K., Malick, K. D., Rabuck, D. A., Raghavachari, K., Foresman, B. J., Cioslowski, J., Ortiz, V. J., Baboul, G. A., Stefanov, B. B., Liu, G., Liashenko, A., Piskorz, P., Komaromi, I., Comperts, R., Martin, L. R., Fox, J. D., Keith, T., Al-Laham, A. M., Peng, Y. C., Nanayakkara, A., Gonzalez, C., Challacombe, M., Gill, W. M. P., Johnson, B., Chen, W., Wong, W. M., Andres, L. J., Head-Gordon, M., Replogle, S. E., and Pople, A. J. (1998) *Gaussian 98*, Gaussian, Inc., Pittsburgh, PA.
34. Bayly, C. I., Cieplak, P., Cornell, W. D., and Kollman, P. A. (1993) A Well-Behaved Electrostatic Potential Based Method Using Charge Restraints for Deriving Atomic Charges: The Resp Model, *J. Phys. Chem. 97*, 10269−80.
35. Jorgensen, W. L., Chandrasekhar, J., Madura, J. D., Impey, R. W., and Klein, M. L. (1983) Comparison of Simple Potential Functions for Simulating Liquid Water, *J. Chem. Phys. 79*, 926−35.
36. Essmann, U., Perera, L., Berkowitz, M. L., Darden, T., Lee, H., and Pedersen, L. G. (1995) A Smooth Particle Mesh Ewald Method, *J. Chem. Phys. 103*, 8577−93.
37. Darden, T., York, D., and Pedersen, L. (1993) Particle Mesh Ewald: An N.Log(N) Method for Ewald Sums in Large Systems, *J. Chem. Phys. 98*, 10089−92.
38. Ryckaert, J. P., Ciccotti, G., and Berendsen, H. J. C. (1977) Numerical-Integration of Cartesian Equations of Motion of a System with Constraints: Molecular-Dynamics of N-Alkanes, *J. Comput. Phys. 23*, 327−41.
39. Harvey, S. C., Tan, R. K. Z., and Cheatham, T. E. (1998) The flying ice cube: Velocity rescaling in molecular dynamics leads to violation of energy equipartition, *J. Comput. Chem. 19*, 726−40.
40. Berendsen, H. J. C., Postma, J. P. M., Vangunsteren, W. F., Dinola, A., and Haak, J. R. (1984) Molecular-Dynamics with Coupling to an External Bath, *J. Chem. Phys. 81*, 3684−90.
41. Case, D. A., Pearlman, D. A., Caldwell, J. W., Cheatham, T. E., III, Wang, J., Ross, W. S., Simmerling, C. L., Darden, T. A., Merz, K. M., Stanton, R. V., Cheng, A. L., Vincent, J. J., Crowley, M., Tsui, V., Gohlke, H., Radmer, R. J., Duan, Y., Pitera, J., Massova, I., Seibel, G. L., Singh, U. C., Weiner, P. K., and Kollman, P. A. (2002) *AMBER 7*, University of California, San Francisco.
42. Saenger, W. (1984) *Principles of Nucleic Acid Structure*, Springer-Verlag, New York.
43. Ravishanker, G., Swaminathan, S., Beveridge, D. L., Lavery, R., and Sklenar, H. (1989) Conformational and helicoidal analysis of 30 PS of molecular dynamics on the d(CGCGAATTCGCG) double helix: "Curves", dials and windows, *J. Biomol. Struct. Dyn. 6*, 669−99.
44. Ravishanker, G., Wang, W., and Beveridge, D. L. (2004) *MD Toolchest*, Wesleyan University, Middletown, CT.
45. Srinivasan, J., Cheatham, T. E., Cieplak, P., Kollman, P. A., and Case, D. A. (1998) Continuum solvent studies of the stability of DNA, RNA, and phosphoramidate: DNA helices, *J. Am. Chem. Soc. 120*, 9401−9.
46. Kollman, P. A., Massova, I., Reyes, C., Kuhn, B., Huo, S., Chong, L., Lee, M., Lee, T., Duan, Y., Wang, W., Donini, O., Cieplak, P., Srinivasan, J., Case, D. A., and Cheatham, T. E., III (2000) Calculating structures and free energies of complex molecules: combining molecular mechanics and continuum models, *Acc. Chem. Res. 33*, 889−97.
47. Wang, W., and Kollman, P. A. (2000) Free energy calculations on dimer stability of the HIV protease using molecular dynamics and a continuum solvent model, *J. Mol. Biol. 303*, 567−82.
48. Reyes, C. M., and Kollman, P. A. (2000) Structure and thermodynamics of RNA-protein binding: Using molecular dynamics and free energy analyses to calculate the free energies of binding and conformational change, *J. Mol. Biol. 297*, 1145−58.
49. Lee, M. R., Duan, Y., and Kollman, P. A. (2000) Use of MM-PB/SA in estimating the free energies of proteins: Application to native, intermediates, and unfolded villin headpiece, *Proteins 39*, 309−16.
50. Wang, J., Morin, P., Wang, W., and Kollman, P. A. (2001) Use of MM-PBSA in reproducing the binding free energies to HIV-1 RT of TIBO derivatives and predicting the binding mode to HIV-1 RT of efavirenz by docking and MM-PBSA, *J. Am. Chem. Soc. 123*, 5221−30.
51. Huo, S., Massova, I., and Kollman, P. A. (2002) Computational alanine scanning of the 1:1 human growth hormone-receptor complex, *J. Comput. Chem. 23*, 15−27.
52. Honig, B., and Nicholls, A. (1995) Classical electrostatics in biology and chemistry, *Science 268*, 1144−9.
53. Nicholls, A., Sharp, K. A., and Honig, B. (1990) *DelPhi*, Department of Biochemistry and Molecular Biophysics, Columbia University, New York.
54. Sitkoff, D., Sharp, K. A., and Honig, B. (1994) Accurate Calculation of Hydration Free-Energies Using Macroscopic Solvent Models, *J. Phys. Chem. 98*, 1978−88.
55. Alberts, B., Bray, D., Lewis, J., Raff, M., Roberts, K., and Watson, J. D. (1994) *Molecular Biology of the Cell*, 3rd ed., Garland Publishing, New York.
56. Gilson, M. K., and Honig, B. H. (1987) Calculation of Electrostatic Potentials in an Enzyme Active-Site, *Nature 330*, 84−6.
57. Sanner, M. F., Olson, A. J., and Spehner, J. C. (1996) Reduced surface: An efficient way to compute molecular surfaces, *Biopolymers 38*, 305−20.

58. Kunkel, T. A. (2004) DNA replication fidelity, *J. Biol. Chem. 279*, 16895−8.
59. Rechkoblit, O., Zhang, Y., Guo, D., Wang, Z., Amin, S., Krzeminsky, J., Louneva, N., and Geacintov, N. E. (2002) trans-Lesion synthesis past bulky benzo[*a*]pyrene diol epoxide N2-dG and N6-dA lesions catalyzed by DNA bypass polymerases, *J. Biol. Chem. 277*, 30488−94.
60. Chiapperino, D., Kroth, H., Kramarczuk, I. H., Sayer, J. M., Masutani, C., Hanaoka, F., Jerina, D. M., and Cheh, A. M. (2002) Preferential misincorporation of purine nucleotides by human DNA polymerase η opposite benzo[*a*]pyrene 7,8-diol 9,10-epoxide deoxyguanosine adducts, *J. Biol. Chem. 277*, 11765−71.
61. Kolbanovskiy, A., Kuzmin, V., Shastry, A., Kolbanovskaya, M., Chen, D., Chang, M., Bolton, J. L., and Geacintov, N. E. (2005) Base selectivity and effects of sequence and DNA secondary structure on the formation of covalent adducts derived from the equine estrogen metabolite 4-hydroxyequilenin, *Chem. Res. Toxicol.* (Web release date, Oct 1, 2005).

BI051090T